Draft version April 24, 2021
Typeset using LaTeX **twocolumn** style in AASTeX631

Is Image D in the Strongly Lensed Quasar SDSS-J0924+0219 in a Zero Micro-Minima State?

Daniel A. Yahalomi[1]

[1]*Department of Astronomy, Columbia University, 550 W 120th St., New York NY 10027, USA*

ABSTRACT

1. INTRODUCTION

1.1. *Gravitational Lensing: Macro and Micro*

General Relativity describes gravity as the warping of space-time. Light travels on the null geodesic in space-time. When a massive galaxy lies between us and a background quasar, it gravitationally lenses the quasar's light, producing multiple images. The mutliplicity of the images can be understood by Fermat's principle, which states that the path that light takes between two points is always a stationary point in time. These stationary points can be determined solving the geometric and gravitational time delays caused by a gravitational lens, where the geometric time delay is due to the additional distance traveled and the gravitational time delay is due to the gravitational warping from the lens mass (Blandford & Narayan 1986):

$$t_{geom}(\theta_I, \theta_S) = \alpha(\theta_I - \theta_S)^2 \tag{1}$$

$$t_{grav}(\theta_I) = 2\alpha(-\psi(\theta_I)) \tag{2}$$

Here, θ_S is the angular position of the source, θ_I is the angular position of the lensed image, α is a constant of the setup (combination of parameters such as distances between the observer, lens, and source, and the redshift), and $\psi(\theta_I)$ is a two-dimensional gravitational potential determined by integrating the three-dimensional gravitational potential along the line of sight (Blandford & Narayan 1986). We can then sum these two contributions to the time delay and set the 2α term to unity to solve for the total time delay in cosmological units (we switch our time variable from t to τ now to note the change in units):

$$\tau_{total}(\theta_I, \theta_S) = \frac{1}{2}(\theta_I - \theta_S)^2 - \psi(\theta_I) \tag{3}$$

Corresponding author: Daniel A. Yahalomi
daniel.yahalomi@columbia.edu

When there is no gravitational potential, $\psi(\theta_I) = 0$ and the only stationary point (a minima) lies at $\theta_I = \theta_S$. However, with a large enough gravitational potential ($\psi(\theta_I) < 0$), multiple stationary points are produced (minima, saddle points, and maxima), which leads to multiple images of the source object. Fermat's principle predicts an odd number of images, and based on the sizes of observed galactic gravitational potentials, we expect either three or five images from strong gravitational lensing. The central image cannot be seen, as it is highly de-magnified by the lensing galaxy, so practically we expect to observe either two or four images (Schneider et al. 2006). For quadruply lensed quasars, we expect to observe two minima and saddle point pairs, which "straddle a critical curve" (Schechter & Wambsganss 2002). These pairs are expected to have roughly the same brightness (Gaudi & Petters 2002; Schechter & Wambsganss 2002).

In reality, the lensing galaxy is not truly a smooth gravitational potential as it is composed of a combination of stars and dark matter. Thus each of the four images of the quasar, seen in quadruply lensed systems (henceforth, macroimages) is in fact the combined observation of many images (henceforth, microimages) created by stars in the lensing galaxy (Paczynski 1986). These stars, that cause these microimages, are called microlenses, and they have characteristic Einstein radii of microarcseconds (μas). These microimages, both in location and brightness, are sensitive to the position of the background quasar relative to a small patch of microlenses that together create the macroimage. Due to the relative motion of the source quasar and the lensing galaxy, the brightness of a macroimage can vary by over an order of magnitude on the short timescale of months or years (Pooley et al. 2019).

As we cannot resolve individual microimages or microlenses, we instead use realizations of the microlensing field using simulations such as the innverse ray shooting method (Wambsganss 1990, 1999), to understand the variability in the macroimage brightness caused by microlensing. Based on a ratio of smooth and clumpy mat-

ter, we can determine how magnified or de-magnified a macroimage would be if the source quasar was located behind a specfic position. These simulations create what we call microlensing magnification map, see Figure 1. The most significant feature in these microlensing magnification maps are called caustics. Whenever a source crosses a caustic, a pair of microimages (a micro-minima and a micro-saddle) are either created or destroyed (Granot et al. 2003). A high-cadence and multi-wavelength observation of such a caustic crossing event could provide information on the nano-arcsecond structure (the same scale as a SMBH) and would produce a rich dataset to map quasar structure (Moustakas et al. 2019). The addition of a micro-image pair created by a caustic crossing event, can be expected to add roughly three times the flux of the unlensed source to the macro-image (Granot et al. 2003; Weisenbach et al. 2019).

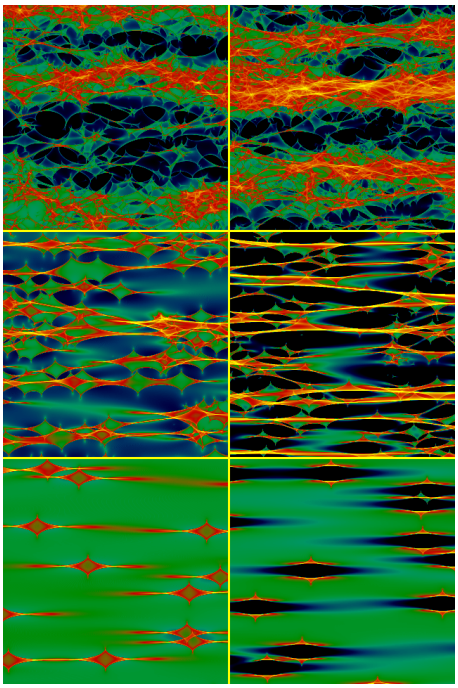

Figure 1. A two-dimensional microlensing magnification map for a typical macro-minimum (on the left) and macro-saddle (on the right) in the quasar plane. Uses stellar contribution to convergence ranging from 100% in the top row, to 15% in the middle row, and to 2% in the bottom row. The color scale ranges from dark blue (large demagnification from microlensing), to light blue, to green, to red, to yellow (large magnification from microlensing). Taken from Schechter & Wambsganss (2002).

1.2. *SDSS J0924+0219*

In their paper's title, Keeton et al. (2006) called SDSS J0924+0219 "the most anomalous lensed quasar." As

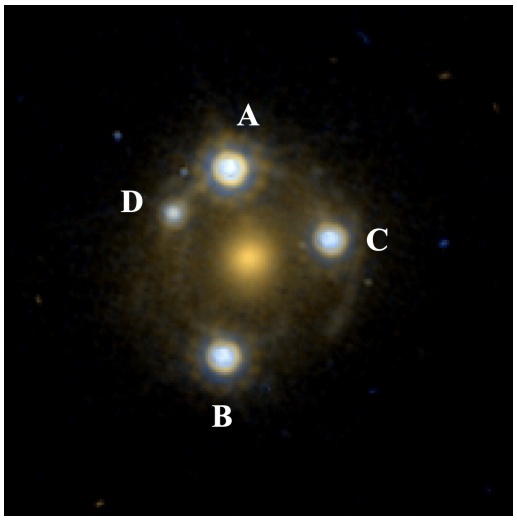

Figure 2. An interpolatted color composite of SDSS J0924+0219 from ACS/WFC from the Hubble Space Telescope. The demagnification of image D is apparent as it is visibly fainter than its pair image *A*.

described above, a generic feature for minima and saddle point pairs in quadruply lensed systems is that these pairs should have approximately equal magnification. In SDSS J0924+0219, images A+D and images B+C are pairs. Inada et al. (2003) measured a flux rato $A/D = 12.5$ in their 2001 December observations with a Sloan i filter and Keeton et al. (2006) measured $A/D = 14.4$ in their 2003 November observations with an F81W filter. As of this writing, image D remains the most extreme example of the suppressed saddlepoint phenomenon discussed by Schechter and Wambsganss (2002). The suppression of image D can be seen by eye in Hubble images from Keeton et al. (2006) in Figure 2.

Mosquera & Kochanek (2011) calculate a timescale $t_E = 20$ yrs for the system's source to traverse the Einstein ring of a micro-lensing star and say "microlensing fluctuations certainly will occur on [this] timescale". Image D has yet to oblige. The possibility that D is gravitationally dimmed by something far more massive than a star, specifically a dark matter subhalo, is ruled out by the recent radio observations of Badole et al. (2020), for which $A/D \sim 1$.

Here we investigate the probability that image D is currently in a state with zero micro-minima. If we can show that image D is in this zero micro-minima state, then we would expect the next caustic crossing event to be particularly propitious for quasar tomography – as the creation of the first micro-minima will have a significant effect on the brightness of the macroimage.

2. CREATING MICROLENSING PROBABILITY DENSITY FUNCTIONS

We can turn the microlensing magnification maps into microlensing probability density functions (PDFs) for magnifications of a specific magnitude. For this project, we assumed $\sim 30\%$ contribution from smooth of the lens in generating the microlensing magnification maps. In what follows, we describe the process in order to create the microlensing PDFs.

The microlensing magnifications maps can be described by a histogram of number of rays vs. the number of pixels with a specific number of rays (henceforth, count). The number of rays have integer bin sizes and we must convert this number of rays to magnitude space. However, in converting to magnitude space, we must convolve the bin sizing to magnitude space. This is necessary as a constant bin sizing in count space is not consistent in magnitude space, which is defined by magnitude $= -2.5\log_{10}(\text{count})$. If we don't do this, then in magnitude space the probability curves for microlensing will have a saw-tooth stepping nature.

In order to do so, we determine the minimum and maximum magnitude from the simulation using the relationship above, and create a grid with a step size of 1/256 magnitudes. We then iterate through the integer bins in number of rays space, convert the integer number of rays to magnitude space and convert the left and right edge (number of rays $\pm$ 0.5) to magnitude space. At each step in this iteration, we add the count to the relevant magnitude bin. If the number of rays integer step spans multiple bins in magnitude space, then we split the total count into the relevant bins by the proportion of the magnitude space bins that the number of rays integer step bin covers.

Once we have successfully converted to magnitude space, we must center the histograms and normalize them. The zero point of the microlensing magnification maps is the mean of the number of pixels. We determine this value for each microlensing magnification histogram and shift the magnitude bins by $+2.5\log_{10}(\text{mean(number of pixels)})$

Next, we normalize the histograms by dividing the counts per magnitude bin by the total area of the histogram, resulting in the microlensing PDFs. We can also follow this same process for image D for only the portions of the micro-magnification maps that have zero micro-minima. The microlensing probability densities can be seen in Figure 3.

image	κ	γ	macro-magnification
A	0.475	0.444	-2.76
B	0.426	0.389	-1.87
C	0.572	0.604	-1.85
D	0.533	0.557	-2.58

Table 1. The κ and γ values used in this paper and the resulting macro-magnification. κ and γ taken from the CASTLES gravitational lens data base (Falco et al. 2001). Note that as described earlier, images A+D and images B+C are pairs of minima and saddle points with similar macro-magnifications.

3. DETERMINING THE UNMAGNIFIED APPARENT MAGNITUDE OF THE QUASAR

Now that we have generated our microlensinig PDFs, we can determine the unmagnifiied apparent magnitude of the quasar (m_{source}). In order to do so, we will take advantage of a set of observations of the four macroimages, a model of the macrolensing magnification values for each image, the microlensing probability densities, and the following equations:

$$\mu_{image} = \frac{1}{detA} = \frac{1}{[(1-\kappa)^2 - \gamma^2]} \tag{4}$$

$$m_{image} = m_{source} - 2.5 * log(|\mu_{image}|) \tag{5}$$

Here, κ (convergence) and γ (shear) are decompositions of the macro-lensing Jacobian (A), determined from the macrolensing model. For this paper, we adopt the following convergence and shear values from the CASTLES gravitational lens data base (Falco et al. 2001). The κ and γ values used and the resulting macro-magnification can be seen in Table 1.

For our observations, we use a set of observations taken in November and provided to us by Paul L. Schechter. We then create a grid of guesses for unmagnified apparent magnitude (m_{source}) with step size of 0.01 magnitudes. By using Equation 5 we can create a grid of macro-predictions of the image magnitude. We then shift each microlensing PDF by the difference between the observed and predicted magnitude of the image. By doing so, the previous zero point now represents the observation of each image. We then multiply together the four microlensing PDFs, which creates a likelihood distribution for microlensing to account for the observed flux ratio anomalies between observed and macro-predicted image brightness. We select the unmagnified apparent magnitude of the quasar that maximizes the resulting likelihood distribution at the observation.

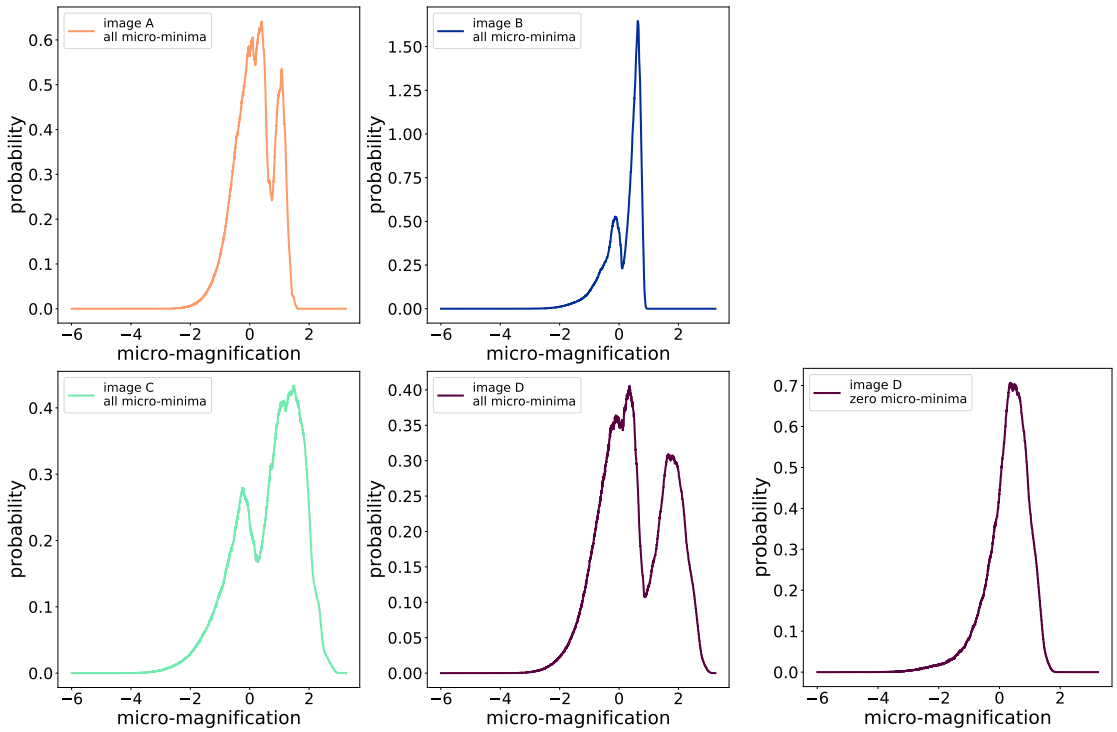

Figure 3. Probability density functions for all four images without any assumptions about the number of micro-minima in the microlensing magnification map. Also shown is the probability density function for image D only for locations in the microlensing magnification map where image D is in a zero micro-minima state.

In determining the unmagnified source of the quasar, we only considered the case where all four images are in the all micro-minima state. Following this procedure, we predict an unmagnified apparent magnitude of 22.29. Figure 4 shows the microlensing PDFs shifted by the difference between their observed magnitudes and macro-predicted magnitudes. The observed magnitude of the four images, macro-predicted magnitude of the four images, and the difference between observed and macro-predicted magnitudes can be seen in Table 2.

As seen in Table 2, our macro-model prediction for image A is 1.197 magnitudes fainter than the observation and our macro-model prediction for image D is 1.634 magnitudes brighter than the observation. Therefore, if microlensing is the cause of these flux ratio anomalies, then it must simultaneously magnify image A by 1.197 magnitudes and de-magnify image D by 1.634 magnitudes.

image	$m_{\rm obs}$	$m_{\rm pred}$	$m_{\rm obs\text{-}pred}$
A	18.314	19.531	-1.197
B	19.891	20.416	-0.505
C	21.071	20.437	0.654
D	21.321	19.707	1.634

Table 2. The observed and macro-predicted magnitudes for all four images.

4. PROBABILITY THAT IMAGE D IS IN A ZERO MICRO-MINIMA STATE

We now evaluate the likelihood that microlensing can account for the differences between observed and macro-predicted brightness of the four images. In order to do so, we take the value of the likelihood function (bottom of Figure 4) at the observation. We evaluate the likelihood for both the all micro-minima state and the zero micro-minima state for image D. By taking the ratio of these two likelihoods, we can determine the probability that image D is in a zero micro-minima state (P(D = 0)), given the assumption that microlensing accounts for the flux ratio anomalies with the macro-predictions. Let us define L(D = 0) as the likelihood that microlensing accounts for the flux ratio anomalies from the macro-predictions and image D is in the zero micro-minima state and L(D = all) as the likelihood that microlensing accounts for the flux ratio anomalies from the macro-predictions and D is in any micro-minima state. With these definition, P(D = 0) can be described by Equation 6.

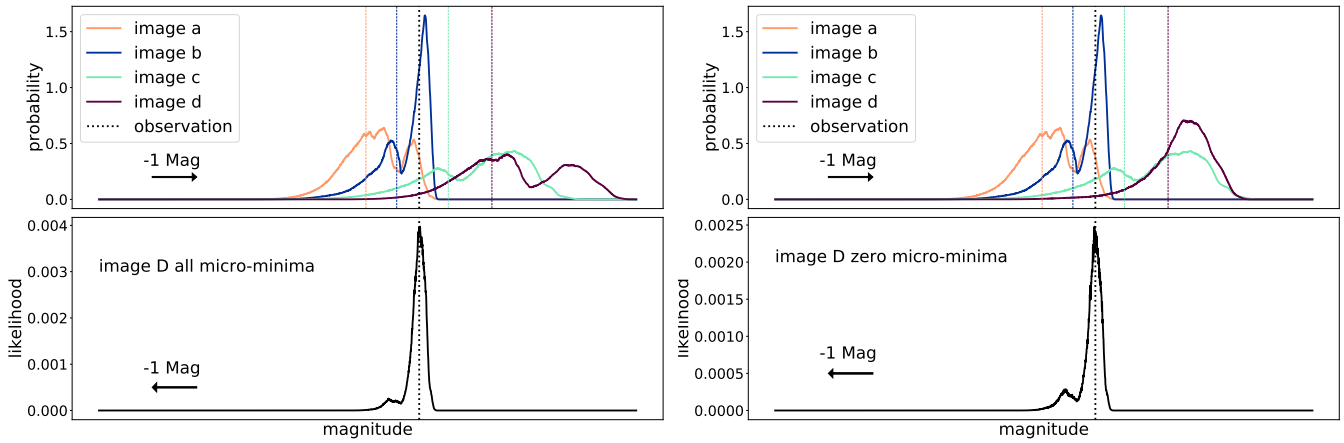

Figure 4. Micro-magnification probability density functions (PDF) for the four images of SDSS J0924+0219 in the top panel. The four probability densities have all been shifted such that the point of zero micro-magnification corresponds to the difference between the observed and macro-predicted flux values. By multiplying the four shifted probability densities, we create a plot that represents the likelihood for microlensing to cause the flux ratio anomalies between observations and macro-predictions as a function of the intrinsic magnitude of the source (bottom panel). On the left is the case where all four images PDFs are derived from the complete microlensing magnification map so any number of micro-minima is allowed. On the right, the PDF of image D is composed from the portion of the microlensing magnification map where there are zero micro-minima.

$$P(D=0) = \frac{L(D=0)}{L(D=\text{all})} \tag{6}$$

Following this procedure, L(D = 0) = 0.00248 and L(D = all) = 0.00397 – therefore we arrive at our result: P(D = 0) = 0.624 or 62.4%.

5. HOW LIKELY IS IT FOR MICROLENSING TO ACCOUNT FOR FLUX RATIO ANOMALIES?

Our probability above is based on the assumption that microlensing accounts for the flux ratio anomalies between macro-predictions and observations. Thus, we would like to test how good is this assumption. In order to do so, we run a 1000 iteration Monte Carlo process. In this Monte Carlo process, we shift the PDF for each image such that the amount of area under the curve to the left of the observation is a random number pulled from a uniform distribution between 0 and 1. We then multiply the 4 PDFs together and determine the likelihood of the resulting product at the observation.

We ran this procedure for 1000 steps for both the zero micro-minima case for image D and the all micro-minima case for image D. The resulting histogram showing the likelihoods vs. count for these two Monte Carlo processes can be seen in Figure 5. We can see that the likelihood that microlensing could produce the requisite flux ratio anomalies between the macro-predictions and observations in this system are both greater then the median likelihood of a random set of flux ratio anomalies. This suggests that there is no reason to be suspicious of microlensing causing the flux ratio anomalies between the macro-predictions and observations.

6. CONCLUSIONS AND FUTURE WORK

In this paper we determined that the probability that image D is in a zero micro-minima state is 62.4%. We also argued that it is not unreasonable to expect for micro-lensing to account for the flux ratio anomalies. However, there is more to be investigated regarding the micro-minima in this system.

Image C is also suppressed in its recent observations relative to its macro-prediction, and thus it is likely that it too is in a zero micro-minima state. We would like to investigate this probability as well.

In addition, rather than comparing the likelihood between zero and all micro-minima for image D (and image C) in determining the probability, we would like to also compare the likelihoods between image D (and image C) being in the zero micro-minima state and the 1 through N micro-minima state. Said differently, we would like to compare the likelihood that the microlensing could account for the flux ratio anomalies under the assumption that image D (and image C) are in the zero micro-minima state vs. NOT in the zero micro-minima state.

In determining this, we would not normalize each probability density by itself, but instead normalize each probability density function of the all micro-minima state. In this setup, we thus wouldn't truly be dealing with probability density functions, and we would have to later worry about scaling in order to determine probability, but it removes possible biases introduced by normalizing the probabilities by such different amounts. Therefore, the probability scale of a cer-

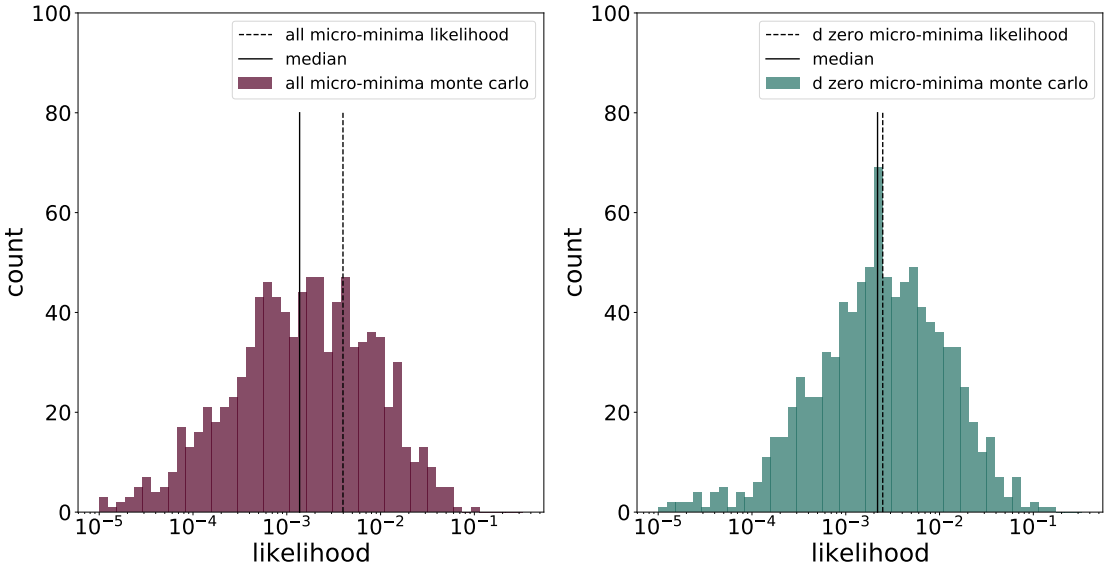

Figure 5. Results of 1000 Monte Carlo simulation for both the all micro-minima case for image D [left] and zero micro-minima case for image D [right]. As we can see, the likelihood required to produce the required flux ratio anomalies between the macro-predictions and observations in this system are both greater then the median likelihood of a random set of flux ratio anomalies.

tain micro-magnification would have a significance on a global scale with the other PDFs rather than just a local scale with itself.

We were surprised that the probability that image D is in the zero micro-minima state was not larger, and are curious if this new procedure will replicate this result or lead to a different conclusion.

7. ACKNOWLEDGMENTS

I would like the thank Paul L. Schechter for the help and guidance with this project. I would also like to thank David Kipping and Adam Wheeler for the all the guidance on this project and throughout this semester in Astrostatistics. This was truly a tremendous class and I truly appreciate all the effort and care that went into running it!

REFERENCES

Badole, S., Jackson, N., Hartley, P., et al. 2020, MNRAS, 496, 138, doi: 10.1093/mnras/staa1488

Blandford, R., & Narayan, R. 1986, The Astrophysics Journal, 310, 568

Falco, E. E., Kochanek, C. S., Lehár, J., et al. 2001, in Astronomical Society of the Pacific Conference Series, Vol. 237, Gravitational Lensing: Recent Progress and Future Go, ed. T. G. Brainerd & C. S. Kochanek, 25

Gaudi, B. S., & Petters, A. O. 2002, ApJ, 574, 970, doi: 10.1086/341063

Granot, J., Schechter, P. L., & Wambsganss, J. 2003, ApJ, 583, 575, doi: 10.1086/345447

Inada, N., Becker, R. H., Burles, S., et al. 2003, AJ, 126, 666, doi: 10.1086/375906

Keeton, C. R., Burles, S., Schechter, P. L., & Wambsganss, J. 2006, ApJ, 639, 1, doi: 10.1086/499264

Mosquera, A. M., & Kochanek, C. S. 2011, ApJ, 738, 96, doi: 10.1088/0004-637X/738/1/96

Moustakas, L., Anguita, T., Chartas, G., et al. 2019, BAAS, 51, 487

Paczynski, B. 1986, The Astrophysics Journal, 301, 503

Pooley, D., Anguita, T., Bhatiani, S., et al. 2019, BAAS, 51, 411. https://arxiv.org/abs/1904.12968

Schechter, P. L., & Wambsganss, J. 2002, The Astrophysics Journal, 580, 685

Schneider, P., Kochanek, C. S., & Wambsganss, J. 2006, Gravitational Lensing: Strong, Weak and Micro (Heidelberg, Germany: Springer-Verlag)

Wambsganss, J. 1990, PhD thesis, J Ludwig-Maximillians-Universitat at Munich

—. 1999, Journal of Computational and Applied Mathematics, 109, 353

Weisenbach, L., Schechter, P., & Wambsganss, J. 2019, MNRAS, 488, 3452, doi: 10.1093/mnras/stz1958